# Interruption of the Internal Water Chain of Cytochrome *f* Impairs Photosynthetic Function[†,‡]

G. Sainz,[§] C. J. Carrell,[||] M. V. Ponamarev,[⊥] G. M. Soriano, W. A. Cramer, and J. L. Smith*

*Department of Biological Sciences, Purdue University, West Lafayette, Indiana 47907-1392*

*Received February 29, 2000; Revised Manuscript Received May 18, 2000*

ABSTRACT: The structure of cytochrome *f* includes an internal chain of five water molecules and six hydrogen-bonding side chains, which are conserved throughout the phylogenetic range of photosynthetic organisms from higher plants, algae, and cyanobacteria. The in vivo electron transfer capability of *Chlamydomonas reinhardtii* cytochrome *f* was impaired in site-directed mutants of the conserved Asn and Gln residues that form hydrogen bonds with water molecules of the internal chain [Ponamarev, M. V., and Cramer, W. A. (1998) *Biochemistry 37*, 17199−17208]. The 251-residue extrinsic functional domain of *C. reinhardtii* cytochrome *f* was expressed in *Escherichia coli* without the 35 C-terminal residues of the intact cytochrome that contain the membrane anchor. Crystal structures were determined for the wild type and three "water chain" mutants (N168F, Q158L, and N153Q) having impaired photosynthetic and electron transfer function. The mutant cytochromes were produced, folded, and assembled heme at levels identical to that of the wild type in the *E. coli* expression system. N168F, which had a non-photosynthetic phenotype and was thus most affected by mutational substitution, also had the greatest structural perturbation with two water molecules (W4 and W5) displaced from the internal chain. Q158L, the photosynthetic mutant with the largest impairment of in vivo electron transfer, had a more weakly bound water at one position (W1). N153Q, a less impaired photosynthetic mutant, had an internal water chain with positions and hydrogen bonds identical to those of the wild type. The structure data imply that the waters of the internal chain, in addition to the surrounding protein, have a significant role in cytochrome *f* function.

Cytochrome $b_6f$ is the electron/proton transfer protein complex of oxygenic photosynthesis that functions between photosystems II and I. Electrons from photosystem II (PS II) are transferred through the Rieske iron−sulfur protein and cytochrome *f* in the high-potential chain of the cytochrome $b_6f$ complex to plastocyanin and photosystem I (PS I). The $b_6f$ complex also contributes to the transmembrane potential via translocation of two protons across the photosynthetic membrane for each electron transferred through the complex. Many aspects and details of the proton translocation pathway are not understood.

Cytochrome *f*, the largest subunit of the $b_6f$ complex, consists of an N-terminal 251-residue redox-active domain in the lumen-side aqueous phase, and a 35-residue C-terminal transmembrane anchor in the photosynthetic membrane of *Chlamydomonas reinhardtii*. The heme in this *c*-type cytochrome is covalently bound to the protein through thioether bonds to Cys21 and Cys24. The spectral and redox properties of the heme, which is ∼45 Å from the transmembrane anchor, are identical in the soluble fragment and in the full-length protein.

The three-dimensional structure of cytochrome *f* is unique among *c*-type cytochromes (*1*). The soluble fragment consists of two $\beta$-domains, the larger of which includes the heme-binding peptide, residues 1−25. The heme Fe is coordinated by the side chain of His25 and the α-amino group of Tyr1. The structure includes a rare buried chain of five water molecules inside the heme-binding large domain (*2*). These structural features are conserved throughout the biological range of cytochrome *f* (*3*). Structures have been reported for cytochrome *f* from turnip (*1*), from the cyanobacterium *Phormidium laminosum* (*3*), and in preliminary form from the alga *C. reinhardtii* (PDB entry 1cfm; *4*).

The function of the buried water chain is unknown. However, residues surrounding the heme and the internal water chain are the most conserved in cytochrome *f*, suggestive of a critical function (*3*). Essentially all residues that form hydrogen bonds with water molecules of the internal buried chain are invariant among at least 27 cytochrome *f* sequences (Figure 1). Only two exceptions to invariance have been reported among residues whose side chains contribute hydrogen bonds to the internal water chain. In the sequence from bean *Vicia faba* (*5*), Thr (codon ACC) is reported at position 153 instead of Asn (possible codon

[†] This work was supported by USDA Grant 98-35306-6405 to J.L.S. and W.A.C. and by NIH Grant GM-38323 to W.A.C.

[‡] Coordinates have been deposited in the Protein Data Bank with access codes 1ewh for the wild type and 1e2v, 1e2z, and 1e2w for the N153Q, Q158L, and N168F variants, respectively.

* Corresponding author. Telephone: (765) 494-9246. Fax: (765) 496-1189. E-mail: smithj@purdue.edu.

[§] Present address: European Synchrotron Radiation Facility, Grenoble, France.

[||] Present address: Department of Biochemistry, Washington University, St. Louis, MO 63110.

[⊥] Present address: Laboratory for Molecular Genetics, National Institute of Environmental and Health Sciences, Research Triangle Park, NC 27709.

10.1021/bi0004596 CCC: $19.00 
Published on Web 07/08/2000

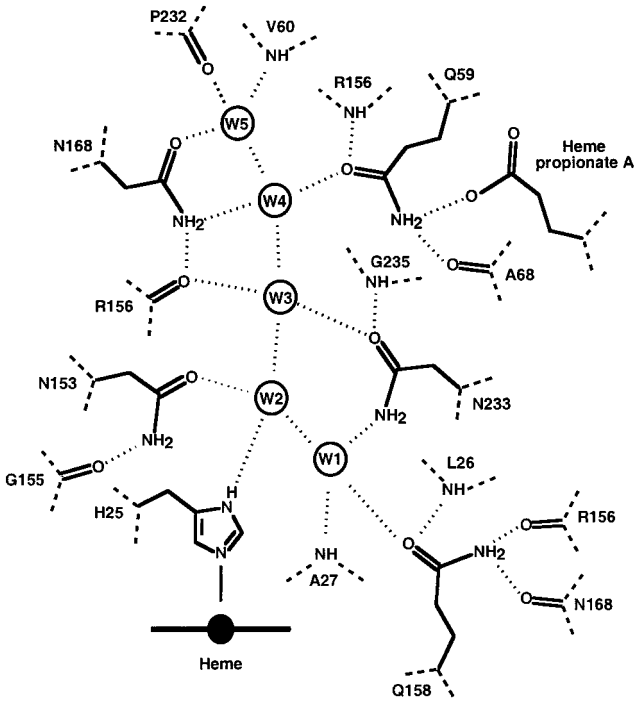


FIGURE 1: Internal water chain of cytochrome *f*. Water molecules W1−W5 are shown in this schematic diagram along with amino acid residues forming hydrogen bonds (dotted lines) with the waters. Covalent bonds in side chains and in backbone carbonyl groups are represented by solid lines and covalent connections between the side chains and the protein backbone as dashed lines. The residue numbering corresponds to *C. reinhardtii* cytochrome *f*.

AAC). In the sequence from the marine diatom alga *Odontella sinensis* (*6*), Ile (codon ATT) is reported at position 168 instead of Asn (possible codon AAT). Large clusters of buried water molecules are rare in proteins (*7*), and are generally associated with a specific function. For example, buried waters have been implicated in the proton transfer pathway of bacteriorhodopsin (*8*) and in the "D channel" for proton uptake in cytochrome oxidase (*9*). The conservation of the internal water chain (*3*) in the proton-pumping $b_6f$ complex implies a role for proton conduction in the exit port of this pump. The pronounced effect on the rate of cytochrome *f* reduction for mutations of conserved residues that contribute side chains to the water chain was interpreted in terms of proton-coupled electron transfer (*10*). However, it has not been possible to obtain isolated coupled membranes on which the effects of these mutations on the proton pump could be tested directly. Therefore, the assignment of the function of the water chain is still unclear.

The function of the water chain in cytochrome *f* was studied in variants in which the water chain was systematically perturbed by mutagenesis. Mutants N153Q, Q158N, Q158L, N168Q, N168F, and N233L were generated in *C. reinhardtii* and the functional consequences characterized (*10*). The most impaired mutant was N168F, which was designed to disrupt the internal water chain and, in fact, could not grow phototrophically. The other mutants grew phototrophically, but did not function as well as the wild type. The major effect in vivo was a pronounced decrease in the rate of cytochrome *f* reduction, greatest in Q158L. The changes in the rate of reduction in vivo in the N153Q and Q158L mutants were also accompanied by a decrease in midpoint potential of 30 and 80 mV, respectively, determined with the soluble form of the cytochrome produced in a heterologous *Escherichia coli* expression system (*10*). Here we present crystal structures for the wild type and three "water mutants" of *C. reinhardtii* cytochrome *f*. The structures of the N153Q, Q158L, and N168F cytochromes were determined in an effort to probe the function of the internal water chain, and to ask whether the loss of phototrophy in N168F and the inhibition of cytochrome *f* function and shift of redox potential in Q158L and N153Q are a consequence of perturbation of the water chain. We find that changes to the structure of the water chain itself are associated with the most severe impairment of cytochrome function.

## MATERIALS AND METHODS

*Purification of Wild-Type Cytochrome f and Plastocyanin from C. reinhardtii via Photoautotrophic Growth.* Plasmid pADI283ST (*11*), provided by F. A. Wollman and R. Kuras, was used to transform the *petA* deletion strain of *C. reinhardtii* (*12*), from R. Malkin and J. Zhou. Cell lines expressing soluble cytochrome *f* were identified and propagated. Purification of soluble cytochrome *f* and plastocyanin from *C. reinhardtii* was carried out as described previously (*10*, *13*). Photoautotrophic growth was carried out at 25−28 °C.

*Heterologous Expression and Purification of Cytochrome f Mutants.* Mutations N153Q and Q158L were generated and recloned into the pUCPF2 construct as previously described (*10*). A polymerase chain reaction (PCR[1])-based protocol was used to generate the N168F mutation in plasmid pUCPF2 (*14*). The pUCPF2 constructs were cotransformed into *E. coli* strain MV1190 (Bio-Rad) with plasmid pEC86 ($Cm^r$), which carries the cassette of cytochrome *c* maturation genes *ccmA*−*H* and was kindly provided by L. Thöny-Meyer (*15*). Transformants were isolated on plates containing ampicillin and chloramphenicol and cultured for expression.

*E. coli* cells used for cytochrome *f* expression were harvested from ∼28 L of culture and osmotically shocked. The yield in the soluble fraction was 1−1.4 mg/L for the wild type and the mutant cytochromes, as determined from the chemical difference spectrum, using a differential extinction coefficient $\Delta\epsilon_{554}$ of 26 $mM^{-1}$ $cm^{-1}$ (*16*). The pink soluble extract was concentrated and dialyzed against 1 mM $Na_2HPO_4/NaH_2PO_4$ buffer (pH 7.5) and loaded on a DEAE-52 Sephacel column. Bound cytochrome *f* was eluted with 100 mM $Na_2HPO_4/NaH_2PO_4$ buffer (pH 7.5) and 1 mM DTT. Combined cytochrome *f* fractions were concentrated to ∼10 mL and passed through a G-100 column, with 10 mM $Na_2HPO_4/NaH_2PO_4$ buffer (pH 7.5). Fractions with an $A_{554}/A_{280}$ ratio of >0.3 were collected, concentrated, and applied to a hydroxyapatite column. Bound cytochrome *f* was washed with 3 volumes of 10 mM $Na_2HPO_4/NaH_2PO_4$ buffer (pH 7.5) and 1 mM DTT and eluted with 100−150 mM $Na_2HPO_4/NaH_2PO_4$ buffer (pH 7.5). Fractions with an $A_{554}/A_{280}$ ratio of >0.9 were combined, concentrated, and stored at −70 °C. The yield of purified cytochrome *f* was ∼20 mg. All protein samples were >95% pure, as judged by SDS−PAGE.

*Crystallization and Diffraction Data Collection.* Purified cytochrome *f* was crystallized at 20 °C by vapor diffusion

[1] Abbreviations: $E_m$, midpoint oxidation−reduction potential; PCR, polymerase chain reaction; PEG, polyethylene glycol; MES, 2-(*N*-morpholino)ethanesulfonic acid; DTT, dithiothreitol; rmsd, root-mean-square displacement.

Table 1: Diffraction Data

| | wild type | N153Q | Q158L | N168F |
|---|---|---|---|---|
| space group | $P2_12_12_1$ | $P2_12_12_1$ | $P2_12_12_1$ | $P2_1$ |
| *a* (Å) | 76.5 | 76.1 | 73.9 | 59.0 |
| *b* (Å) | 94.3 | 94.2 | 94.7 | 81.2 |
| *c* (Å) | 119.9 | 121.1 | 122.6 | 61.1 |
| $\beta$ (deg) | − | − | − | 103.5 |
| diffraction data | | | | |
| X-ray source | CuKα | APS ID14B | APS BM14C | APS ID19 |
| wavelength (Å) | 1.5418 | 1.0000 | 1.0000 | 0.6526 |
| X-ray detector | R-axis IP | Q4 CCD | Q4 CCD | 3 × 3 CCD |
| data range (Å) | 50.0−2.35 | 43.85−1.85 | 47.14−2.50 | 27.84−1.60 |
| completeness (%) | 95.2 (91.0)[a] | 97.9 (90.2) | 97.1 (73.1) | 99.6 (100) |
| $R_{sym}$[b] (%) | 5.9 (26.3) | 4.8 (30.5) | 7.8 (20.1) | 4.60 (37.8) |
| average $I/\sigma_I$ | 19.5 (3.6) | 26.1 (3.7) | 22.7 (4.6) | 28.6 (3.5) |
| no. of observations | 128030 | 329989 | 162713 | 277890 |
| no. of unique reflections | 35044 | 73484 | 29632 | 73580 |
| average redundancy | 3.7 | 4.5 | 5.5 | 3.8 |

[a] Values in parentheses pertain to the outermost shell of data. [b] $R_{sym} = \Sigma_{hj}|I_h - I_j|/\Sigma_j I_j$, where $I_h$ is the average intensity for all observations of a reflection with unique indices *h* and $I_j$ is the *j*th observation of a reflection with average intensity $I_h$.

in droplets containing equal volumes of 10 mg/mL protein solution and reservoir. All cryoprotected crystals were immediately flash-frozen at 100 K in an Oxford Cryosystems cold $N_2$ stream. The wild-type cytochrome *f* solution included 88 mM $Na_2HPO_4/NaH_2PO_4$ buffer (pH 7.5) and 1 mM DTT, and the reservoir was 100 mM MES (pH 6.5), 25−50 mM calcium acetate, and 12−18% (w/v) PEG 8000 (Fluka). Small rod crystals (200 $\mu$m × 80 $\mu$m × 50 $\mu$m) were harvested into 100 mM MES (pH 6.5), 25 mM calcium acetate, and 15% PEG 8000 and cryoprotected in 20 min by transfer through harvesting solutions with successively higher concentrations of glycerol in increments of 4% to a final concentration of 20%. The N153Q cytochrome *f* solution included 80 mM $Na_2HPO_4/NaH_2PO_4$ buffer (pH 7.5) and 1 mM DTT, and the reservoir was 100 mM MES (pH 6.5), 25 mM calcium acetate, 1 mM DTT, and 17−19% PEG 8000. Crystals were grown for 4 days at 12 °C and then at 20 °C. Rectangular plate crystals (240 $\mu$m × 200 $\mu$m × 80 $\mu$m) were harvested into 100 mM MES (pH 6.5), 25 mM calcium acetate, and 18% PEG 8000 and cryoprotected by transfer through harvesting solutions with successively higher concentrations of glycerol in increments of 6% to a final concentration of 25%. The Q158L cytochrome *f* solution included 10 mM $Na_2HPO_4/NaH_2PO_4$ buffer (pH 7.5) and traces of DTT, and the reservoir was 100 mM MES (pH 6.7), 50 mM ammonium fluoride, 5% glycerol, and 19−21% PEG 3350 (Hampton). A crystal (250 $\mu$m × 100 $\mu$m × 80 $\mu$m) was cryoprotected by harvesting into 100 mM MES (pH 6.7), 50 mM ammonium fluoride, 15% glycerol, and 21% PEG 3350 for 15 s. The N168F cytochrome *f* solution included 10 mM $Na_2HPO_4/NaH_2PO_4$ buffer (pH 7.5) and 1 mM DTT, and the reservoir was 100 mM MES (pH 6.7), 200 mM ammonium formate, 14% glycerol, and 17% PEG 3350. A crystal (280 $\mu$m × 200 $\mu$m × 80 $\mu$m) was harvested into 100 mM MES (pH 6.7), 200 mM ammonium formate, 14% glycerol, and 21% PEG 3350 and cryoprotected in 10 min by transfer through harvesting solutions with 15, 18, 21, and 25% glycerol.

X-ray diffraction data for the wild-type cytochrome were recorded with CuKα radiation using a Rigaku RU-200 rotating anode source and a Rigaku R-Axis IV image plate detector (Molecular Structures Corp.) in a single 100° sweep of 1° oscillation images. Data for the N153Q mutant cytochrome were recorded using the wiggler source at BioCARS beam line ID14-B at the Advanced Photon Source (APS) on a Quantum 4 2 × 2 mosaic CCD detector (Area Detector Systems Corp.) in a single 233° sweep of 1° oscillation images. Data for the Q158L mutant cytochrome were recorded using the bending-magnet source at BioCARS beam line BM14-C at the APS on a Quantum 4 CCD detector in a 118° high-resolution sweep of 0.5° oscillation images at 60 s exposure and an 85° low-resolution sweep of 1.5° oscillation images at 10 s exposure. Data for the N168F mutant cytochrome were recorded using the undulator source at SBC beam line ID19 at the APS on a 3 × 3 mosaic CCD detector (*17*) in 180° sweeps of 1° oscillation images of 10 s at high resolution and 2° oscillation images of 2 s at low resolution. Data were processed with the HKL package (*18*, *19*) and are summarized in Table 1.

*Structure Determination and Refinement.* The structure of wild-type *C. reinhardtii* cytochrome *f* was determined by molecular replacement from a truncated model of the 70% identical turnip cytochrome *f* (PDB entry 1hcz; *2*) using the program AMoRe (*20*, *21*). After positioning of the three cytochrome *f* molecules in the asymmetric unit and rigid-body refinement in AMoRe using 20−4.0 Å data, the truncated model had a correlation coefficient of 0.59 and an *R*-factor of 0.41. The truncated model was completed to reflect the sequence of *C. reinhardtii* cytochrome *f*. All manual model building and inspection were carried out with the program O (*22*). The complete model was refined in stages using the program CNS (*23*): rigid-body refinement of large and small domains, grouped *B*-factor refinement (two thermal parameters per residue, for side chain and main chain atoms), simulated annealing, and several rounds of positional and individual atomic *B*-factor refinement alternating with manual model building. Waters were identified using the automatic procedure in the CNS program, which is based on peak picking in $|F_o| - |F_c|$ maps and iterative acceptance and/or rejection by geometric criteria. The ordered solvent structure for all refined models was verified by inspection.

The refinement protocol for the mutant cytochrome *f* structures was similar to that used for the wild type, without the simulated annealing step. At each site of mutation, side chain atoms beyond $C_\beta$ were deleted from the starting model. All ordered solvent molecules, including the five internal

Table 2: Summary of Refined Cytochrome *f* Models

| | wild type | N153Q | Q158L | N168F |
|---|---|---|---|---|
| model refinement | | | | |
| data range (Å) | 50−2.35 | 43.85−1.85 | 47.14−2.50 | 27.84−1.60 |
| data cutoff | $\|F\| > 0$ | $\|F\| > 0$ | $\|F\| > 0$ | $\|F\| > 0$ |
| $R_{work}$[a] (%) | 18.7 | 18.5 | 21.2 | 19.7 |
| no. of reflections | 31439 | 67793 | 27344 | 67515 |
| $R_{free}$[a] (%) | 25.6 | 21.9 | 27.9 | 22.6 |
| no. of reflections | 2773 | 3635 | 1475 | 3704 |
| overall anisotropic *B* factors (Å$^2$) | | | | |
| $B_{11}$ | −6.2 | −2.4 | −6.7 | 1.3 |
| $B_{22}$ | 2.2 | −2.0 | 3.6 | −0.6 |
| $B_{33}$ | 4.0 | 4.5 | 3.2 | −0.7 |
| $B_{13}$ | − | − | − | 1.7 |
| refined model | | | | |
| residues | 1−251 | 1−251 | 1−251 | 1−251 |
| no. of protein atoms | 6602 | 5751 | 5745 | 3832 |
| no. of solvent atoms | 721 | 1160 | 278 | 757 |
| average *B* (Å$^2$) | | | | |
| main chain | 30.1 | 23.3 | 45.6 | 21.5 |
| side chain | 33.5 | 30.4 | 49.7 | 24.9 |
| water | 42.9 | 40.4 | 44.6 | 38.2 |
| heme | 17.7 | 13.8 | 31.5 | 14.0 |
| all atoms | 31.7 | 28.8 | 47.1 | 28.8 |
| rms deviations from target values | | | | |
| bond lengths (Å) | 0.010 | 0.005 | 0.007 | 0.005 |
| bond angles (deg) | 1.65 | 1.32 | 1.40 | 1.34 |
| *B* factors of bonded atoms (Å$^2$) | 3.1 | 4.2 | 4.7 | 2.0 |
| estimated coordinate error (Å) | | | | |
| Luzzati | 0.25 | 0.20 | 0.35 | 0.18 |
| SigmaA | 0.18 | 0.14 | 0.28 | 0.13 |

[a] $R = \Sigma||F_o| - |F_c||/\Sigma|F_o|$. A random 5−8% subset of the data was used for the $R_{free}$ calculation.

waters, were also deleted. In each case, electron densities for the mutant side chain and for the internal waters were clear in the first $|F_o| - |F_c|$ map. Crystals of N153Q and wild-type cytochrome *f* were nearly isomorphous, and the wild type was used as a starting model. Several residues were modeled in dual conformations: Leu51, Ile130, and Val141 in chain A, Ile19 and Ile130 in chain B, and Ser142, Val159, and Ile215 in chain C. The last iteration of refinement was followed by one round of atomic occupancy refinement for residues in dual positions. Three strong electron density peaks were interpreted as acetate ions from the crystallization solution. Crystals of Q158L cytochrome *f* were also nearly isomorphous with those of the wild type and the N153Q cytochrome. The 1.9 Å structure of N153Q cytochrome *f* was used as a starting model for refinement of the Q158L mutant structure. No residues in dual positions were visible in the lower-resolution maps of Q158L cytochrome *f*, and fewer water molecules were identified. Atomic *B*-factors from the N153Q starting model were retained, but adjustments were made only through the grouped *B*-factor refinement procedure in CNS. In the last round of refinement, individual atomic *B*-factors were refined for Leu158. Crystals of N168F cytochrome *f* were not isomorphous with the others, and the structure was determined by molecular replacement from the 1.9 Å structure of N153Q cytochrome *f* using the program AMoRe. After positioning of the two cytochrome *f* molecules in the asymmetric unit and rigid-body refinement in AMoRe using 15−3.5 Å data, the correlation coefficient was 0.44 and the *R*-factor was 0.41 for a model that was complete except for the side chain at position 168. In the final model, dual positions were modeled for Leu19, Val39, Leu75, Ile93, Val141, and Val159 in chain A and for Cys21 and Glu79 in chain B. The last iteration of refinement was followed by one round of atomic occupancy refinement for residues in dual positions. The refined models are summarized in Table 2.

*Structure Comparisons.* Structure comparisons were carried out as for plant and cyanobacterial cytochrome *f* (*3*). $C_\alpha$ atoms in the large domain of *C. reinhardtii* cytochrome *f* (residues 1−169 and 231−249) were superimposed using routines in the program O and the program LsqKab in the CCP4 suite (*24*). All structure comparisons were based on superpositions that in no instance included the buried water chain. For the multiple copies of cytochrome *f* in each crystal structure, analogous water positions in the buried water chains were identical within experimental error following the large-domain $C_\alpha$ superposition, except where otherwise noted. Therefore, an average water position at each of the buried sites was used in the analysis.

*Spectroscopy and Determination of Cytochrome f Midpoint Potential.* Spectroscopic measurements were taken using a Cary UV−visible spectrophotometer (Varian). The precision (±0.1 nm) of the wavelength calibration was checked using the 486.0 and 656.1 nm emission lines of an internal deuterium lamp. Midpoint oxidation−reduction potentials for the wild type and mutant forms of cytochrome *f* were determined by titration with ferri- and ferrocyanide at pH 7.0 in 50 mM $K_2HPO_4/KH_2PO_4$ buffer while monitoring the redox potential and the absorbance at 554 nm. The initial potential (ca. 500 mV) was set by addition of 0.5 mM potassium ferricyanide and the titration carried out by subsequent addition of aliquots of sodium ascorbate to decrease the potential in 15−20 mV decrements. The potential at each point of the titration was measured with a digital multimeter (Fluke 73 Series II). The electrochemical cell consisted of a Pt wire with an Ag/AgCl electrode (MF

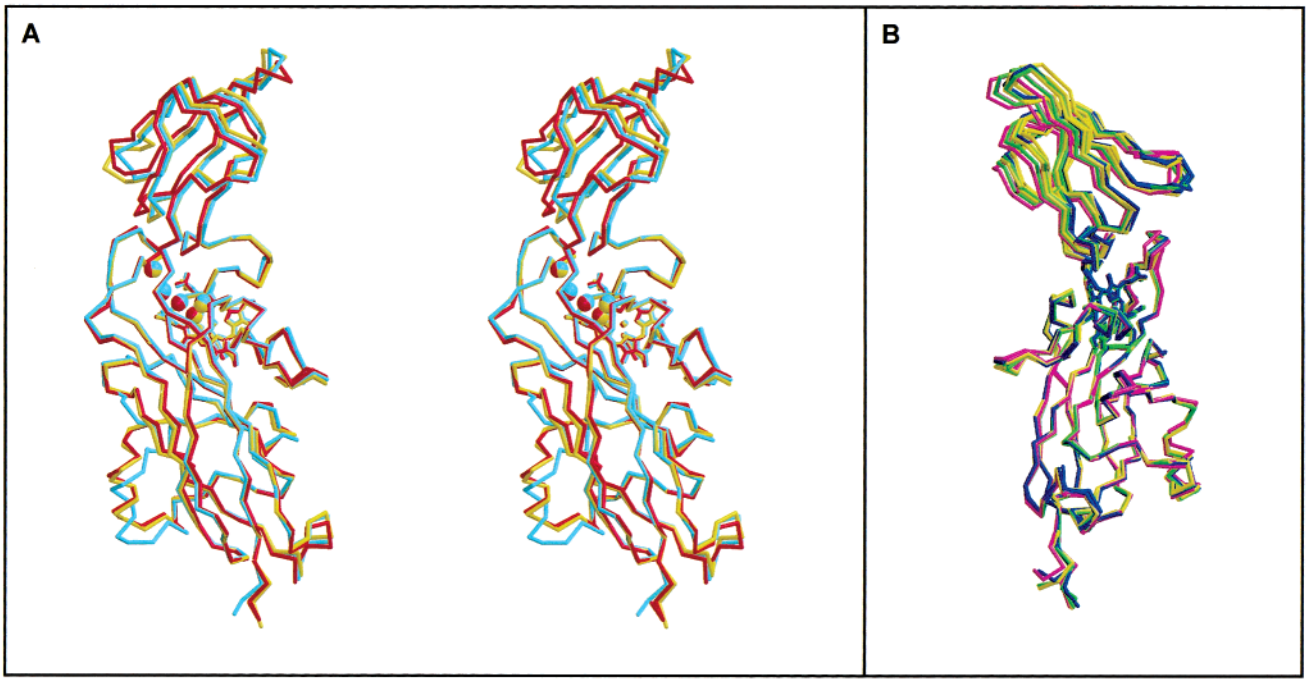


FIGURE 2: Comparison of cytochrome *f* structures. (A) Comparison of structures of algal, plant, and cyanobacterial cytochrome *f*. The $C_\alpha$ atoms of the large domains of *C. reinhardtii* (yellow), turnip (red), and *P. laminosum* (cyan) cytochrome *f* are superimposed in this stereo $C_\alpha$ trace of the polypeptide. The large domain is shown with bound heme. The small domain is at the top of the diagram. The soluble fragment C-terminus, which is connected to the transmembrane domain in the full-length protein, is at the bottom. The buried chain of five water molecules is depicted as spheres. (B) Flexible hinge between domains of cytochrome *f*. All copies of all variants of *C. reinhardtii* cytochrome *f* are shown following superposition of the $C_\alpha$ atoms of the large domains. Flexibility between the domains is apparent in the spread of positions of the small domains. This view is from the back relative to that in panel A. Wild-type cytochrome *f* is drawn in yellow (three copies), N153Q in green (three copies), Q158L in blue (three copies), and N168F in magenta (two copies).

2052 microelectrode, Bioanalytical Systems) as a reference ($E_{ref}$ = 210−220 mV). The potential of the Ag/AgCl electrode was calibrated versus a saturated solution of quinhydrone (*25*). The titration was fit to a one-electron Nernst equation.

*Stopped-Flow Kinetics of Cytochrome f Oxidation by Plastocyanin.* The kinetics of cytochrome *f* oxidation by plastocyanin in solution were studied using a stopped-flow spectrophotometer (Applied Photophysics SX.18MV), in 2 mM $K_2HPO_4/KH_2PO_4$ buffer (pH 7.0) and 0.2 M NaCl. The concentration of cytochrome *f*, which was purified from the *E. coli* expression system, was 0.1 $\mu$M in the 200 $\mu$L reaction mixture, and that of plastocyanin was 10, 15, and 20 times greater for realization of pseudo-first-order kinetics for the oxidation. The rate of cytochrome oxidation was monitored as the rate of decrease in absorbance at the corresponding peaks of the Soret band of the reduced cytochrome. The pseudo-first-order kinetic data were fit with a single exponential to obtain the first-order rate constant, $k_{obs}$ ($s^{-1}$). The resulting $k_{obs}$ values were plotted against plastocyanin concentration to obtain the bimolecular rate constant, $k_2$ ($M^{-1}$ $s^{-1}$).

## RESULTS

*Structures of Wild-Type and Mutant C. reinhardtii Cytochrome f.* The crystal structures of wild-type and mutant *C. reinhardtii* cytochrome *f* offer a total of 11 views of the protein in five different crystal environments. Crystals of the wild-type, N153Q, and Q158L cytochromes were nearly isomorphous, each with three molecules in the crystallographic asymmetric unit. The N168F variant produced a different crystal form with two independent molecules. The quality of the four structures is correlated with the diffraction limits of the crystals, as is evident in the average temperature factors, the number of ordered water molecules per polypeptide, and the estimated coordinate errors (Table 2). The best diffraction data were obtained for the N168F cytochrome by collimating the undulator X-ray beam to irradiate only one well-formed end of the crystal. The Q158L variant was recalcitrant to crystallization and produced more weakly diffracting crystals than the other variants. Crystals of all variants except N168F exhibited anisotropic diffraction; anisotropy was most severe for the wild-type and Q158L crystals. Each structure includes all 251 residues encoded by the construct used for expression. No residues are found in disallowed regions of the Ramachandran plot apart from the small-domain loop of residues 187−189 and the C-terminus, which are less well ordered than the rest of the molecule in all crystal structures. Residues 249−251, which are connected to the transmembrane domain in the full-length protein, adopt a variety of conformations in the four crystal structures, and are involved in lattice contacts in several instances. For each crystal structure, differences among redundant copies of the protein are nearly at the level of experimental error. These intracrystal differences were used to evaluate differences between wild-type and mutant cytochromes.

*Comparison of C. reinhardtii, Plant, and Cyanobacterial Cytochromes f.* The structure of *C. reinhardtii* cytochrome *f* is very similar to structures of the plant and cyanobacterial cytochromes, as expected for proteins with sequences more than 60% identical. $C_\alpha$ atoms of the wild-type *C. reinhardtii*

Table 3: Oxidation−Reduction Potentials and Spectral Parameters of Wild-Type and Mutant *C. reinhardtii* Cytochrome *f*

| | | | Soret band $\lambda_{max}$ (nm) | |
|---|---|---|---|---|
| | $E_m$ (mV)[a] | α-band $\lambda_{max}$ (nm) | reduced | oxidized |
| wild type[b] | 373 ± 3 (2)[c] | 554.1 ± 0.2 | 421.1 ± 0.2 | 410.0 ± 0.4 |
| N153Q[b] | 342 ± 3 (3) | 555.0 ± 0.2 (549)[d] | 420.7 ± 0.2 | 407.0 ± 0.4 |
| Q158L[b] | 294 ± 6 (2) | 553.7 ± 0.2 | 420.6 ± 0.2 | 407.6 ± 0.4 |
| N168F | 342 ± 6 (2) | 553.4 ± 0.2 | 421.0 ± 0.2 | 408.8 ± 0.4 |

[a] Measured vs the Ag/AgCl electrode at pH 7.0. [b] From ref *10*. [c] Number of experiments. [d] Major secondary peak in parentheses.

Table 4: Kinetic Parameters for Wild-Type and Mutant Forms of *C. reinhardtii* Cytochrome *f*

| | | cytochrome *f*[a] | | | |
|---|---|---|---|---|---|
| | culture doubling time[a] (h) | $t_{1/2}$ for oxidation (μs) | $t_{1/2}$ for reduction (ms) | slow $\Delta\psi$[a] $t_{1/2}$ (ms) | in vitro oxidation by plastocyanin $k_2$ ($\times 10^7$ $M^{-1}$ $s^{-1}$) |
| WT | 5.1 ± 0.4 | 220 ± 47 | 6 ± 2 | 6 ± 1 | 62 |
| N153Q | 7.5 ± 0.7 | 237 ± 56 | 27 ± 8 | 11 ± 3 | 52 |
| Q158L | 9.7 ± 0.8 | 383 ± 74 | 38 ± 10 | 18 ± 3 | 73 |
| N168F | | nd[b] | nd | nd | 73 |

[a] From ref *10*. [b] Not determined due to insufficient levels of cytochrome $b_6f$ in vivo.

large domains superimpose with those of the turnip cytochrome (*1*) with an average rmsd of 0.5 Å, and with those of the cyanobacterial cytochrome (*3*) with an average rmsd of 0.8 Å (Figure 2A). The small domains of the algal, plant, and cyanobacterial cytochromes are likewise similar (data not shown).

A flexible hinge connects the large and small domains of *C. reinhardtii* cytochrome *f* (Figure 2B). The hinge angle differs by 3−6° among the three independent molecules of the wild-type cytochrome, and by about the same amount between the wild-type and mutant cytochromes (3−8°). Thus, individual cytochrome variants display no preference for a particular hinge position (Figure 2B). Even greater flexing of the hinge may occur in solution. A flexible hinge was inferred from the 4.5° difference between small domain positions in the cyanobacterial and turnip cytochromes (Figure 2A), but interspecies differences could not be ruled out (*3*).

*Spectroscopic and Redox Properties of the Cytochrome f Mutants.* The oxidation−reduction midpoint potential ($E_m$) and spectral parameters were measured in *E. coli* extracts for the N168F non-phototrophic mutant of *C. reinhardtii* cytochrome *f*. In Table 3, these values are compared with previously reported values for the wild type and the N153Q and Q158L variants (*10*). Spectral parameters include the wavelength maxima of the Soret band in the visible spectrum and of the Q-band (α-band) in the difference spectrum of reduced minus oxidized cytochrome *f*. Rates of cytochrome *f* oxidation by plastocyanin in solution were measured using purified proteins and are presented in Table 4 along with previously reported in vivo kinetic parameters for the wild type and phototrophic variants (*10*).

A 30−80 mV decrease in $E_m$ relative to that of the wild type was observed in the mutant cytochromes, with the Q158L variant exhibiting the largest change. The $E_m$ of 342 mV for the non-phototrophic N168F variant was less positive than the wild-type value by only 30 mV ($\Delta E_m = -30$ mV). The phototrophic mutants N153Q and Q158N exhibited approximately the same $\Delta E_m$ as N168F, whereas two other phototrophic mutants, N168Q and Q158L, had larger decreases in $E_m$ to values of 314 and 294 mV, respectively (*10*). Thus, an altered redox potential could not explain the non-phototrophic phenotype resulting from the N168F mutation.

The spectral characteristics of the mutant proteins were changed slightly compared to those of the wild type (Table 3). The Q-band (α-band) peaks of the reduced and oxidized spectra of the Q158L and N168F mutants were blue-shifted by 0.3 and 0.6 nm, respectively, with spectral reproducibility of ±0.1 nm. The largest spectral shift was in the peak of the N153Q mutant, which was red-shifted by ∼1 nm and had an additional shoulder at 549 nm. Compared to those of the wild-type protein, the Soret peaks of the reduced forms of the three mutant proteins were virtually unchanged, whereas the spectra of the oxidized forms were blue-shifted by 1.2−3 nm.

The phototrophic cytochrome $b_6f$ complexes of *C. reinhardtii* containing the N153Q and Q158L mutant forms of cytochrome *f* displayed altered kinetic properties in vivo (Table 4). Compared to the wild type, these cells exhibited 4−6-fold slower rates of cytochrome *f* re-reduction following rapid oxidation induced by a light flash. The slow (milliseconds) formation of a membrane potential ($\Delta\psi_s$) in thylakoid membranes, which is attributed to net charge transfer through the cytochrome $b_6f$ complex, was also affected by the mutations. The absorbance spectrum of membrane-associated carotenoid molecules undergoes a spectral shift with a change in the membrane potential, which gives rise to the so-called "electrochromic bandshift". The half-times for the rise of the slow electrochromic bandshift were increased by factors of 2 and 3 in mutants N153Q and Q158L, respectively. No electrochromic bandshift was detected for cells containing N168F cytochrome *f* even when they were grown heterotrophically; there was no phototrophic growth. As noted above, the data for mutant cytochromes also do not indicate a correlation between changes in the $E_m$ values and the rates of reduction for the mutant proteins. For example, although Q158L has the largest $\Delta E_m$ and slowest rate of reduction in vivo, no correlation was observed between the $\Delta E_m$ and the reductive rate for the three conservative mutants (N168Q, N153Q, and Q158N) and the nonconservative mutant N233L (*10*).

Rate constants for the oxidation of cytochrome *f* by *C. reinhardtii* plastocyanin were measured in vitro using purified cytochrome *f* that was produced in *E. coli*. The second-order rate constant was not significantly changed when mutant proteins N153Q ($52 \times 10^7$ $M^{-1}$ $s^{-1}$) and Q158L ($73 \times 10^7$ $M^{-1}$ $s^{-1}$) were used in the reaction as opposed to the wild type ($60 \times 10^7$ $M^{-1}$ $s^{-1}$). A similar rate was also measured with the N168F mutant protein ($73 \times 10^7$ $M^{-1}$ $s^{-1}$). Thus, the non-phototrophic phenotype of the N168F mutant is not a consequence of a large decrease in the rate of electron transfer to plastocyanin, and must be associated with other functions of cytochrome *f* within the $b_6f$ complex. However, it should be noted that the bimolecular rate for the cytochrome *f*−plastocyanin reaction in vitro, which was measured by stopped-flow spectroscopy, is limited by the association kinetics of cytochrome *f* and plastocyanin rather than by the rate of interprotein electron transfer.

Table 5: Structural Similarity of Wild-Type and Mutant *C. reinhardtii* Cytochrome *f*

| | wild type | | | N153Q | | | Q158L | | | N168F | |
|---|---|---|---|---|---|---|---|---|---|---|---|
| | A | B | C | A | B | C | A | B | C | A | B |
| wild-type A[a] | − | 0.38 | 0.41 | 0.23 | 0.40 | 0.37 | 0.33 | 0.48 | 0.45 | 0.40 | 0.57 |
| N168F A[a] | 0.40 | 0.34 | 0.38 | 0.36 | 0.33 | 0.33 | 0.37 | 0.39 | 0.44 | − | 0.19 |

[a] The rmsd (angstroms) of 188 large-domain $C_\alpha$ atoms of all molecules in all four crystal structures superimposed with molecule A of the wild-type and N168F *C. reinhardtii* cytochrome *f*.

*Structure Comparisons of Wild-Type and Mutant C. reinhardtii Cytochrome f.* All comparisons were based on superposition of the 188 $C_\alpha$ atoms in the large domain of each independent cytochrome *f* from each crystal structure onto molecule A of the N168F cytochrome structure (Table 5). The N168F variant was used as the superposition standard because it produced the highest-quality crystal structure. The similarity of multiple, independent copies of cytochrome *f* in each of the crystal structures provided a metric against which to evaluate the differences between wild-type and mutant cytochromes. In general, large domains of the wild type and N153Q, Q158L, and N168F variants superimposed as well with each other (0.2−0.6 Å rmsd) as the redundant copies of cytochrome *f* superimposed within each crystal structure (0.3−0.6 Å rmsd). We used a similar approach to compare the buried water chains in the four cytochrome *f* crystal structures. Although they were not used to determine the superposition operator, the water molecules of the internal chain superimposed as well as the $C_\alpha$ atoms within each crystal structure. Because the discrepancy of internal water positions within each crystal structure was not significantly greater than the estimated error in atomic positions, an average water position at each site in the internal chain was used to compare mutant and wild-type structures. These average positions are depicted in Figure 3, and a quantitative summary is given in Table 6.

*N153Q.* The amide group of Gln153 in N153Q cytochrome *f* occupies the same site and has the same hydrogen bonding interactions as the Asn153 amide in the wild-type cytochrome (Figures 1 and 3A). The Gln153 side chain is 0.5 Å closer to the heme than Asn153 due to the extra methylene group. This slight perturbation of the heme environment may account for the spectroscopic changes of this mutant.

*Q158L.* The amide side chain of Gln158 in wild-type cytochrome *f* occupies a polar pocket in the structure and forms hydrogen bonds with three main chain atoms (Leu26 NH, Arg156 O, and Asn168 O) and with W1 of the internal water chain. Leu158 cannot satisfy these hydrogen bonds, and the Leu substitution causes a major local perturbation in the structure (Figures 1 and 3B). The Leu158 side chains have different conformations in the three independent cytochrome molecules and higher temperature factors than the Gln158 side chains in the wild-type structure. Multiple Leu158 conformations are not evident in any of the three independent molecules, but it is unlikely that low-occupancy conformers would be visible in the electron density at 2.5 Å resolution. The Leu158 side chains in two of the cytochrome *f* molecules (A and C) point toward the internal water chain. There is no density at the W1 position in molecule C, for which Leu158 is nearest the water chain. In molecule A, W1 is displaced nearly 1 Å from its position in all other *C. reinhardtii* cytochrome *f* molecules. In molecule B, with the distal Leu158, W1 occupies a position analogous to W1 in the other variants. We conclude that in solution, Leu substitution at position 158 results in weaker binding of water at the W1 position.

*N168F.* Two of five water molecules were lost from the internal water chain in N168F. The amide side chain of Asn168 in wild-type cytochrome *f* is hydrogen bonded through $N_{\delta 2}$ to W4 and through $O_{\delta 1}$ to W5 of the internal water chain (Figure 1). The aromatic ring of Phe168 in N168F cytochrome *f* displaces the two water molecules and occupies the same space as $N_{\delta 2}$, $O_{\delta 1}$, W4, and W5 in the wild-type structure (Figure 3C). Consequently, the Phe side chain has close contacts with polar atoms in the water pocket, including Val60 N, Arg156 O, Pro232 O, and Asn233 $O_{\delta 1}$.

*Changes in the Internal Water Chain.* The largest change in the structure of the internal water chain is the loss of W4 and W5 in the N168F cytochrome. The Phe168 side chain of N168F occupied the positions of W4 and W5 in the wild-type protein. A much smaller change is seen in the Q158L cytochrome, where the occupancy of the water in position W1 is reduced to the point of vanishing from one of three independent molecules and significantly shifted in a second. We quantitated changes in the internal water structure between wild-type and mutant cytochromes, using water positions averaged over the redundant copies in each crystal structure (Table 6). The internal water structure is remarkably well preserved, except sites where waters have been displaced. Overall, changes in water positions between mutant and wild-type structures are smaller than the estimated error in atomic positions. The internal water chain is part of the most well ordered core of the structure for mutants and the wild type alike. The temperature factors for the internal water molecules are lower than the average temperature factor of protein main chain atoms in all cases.

## DISCUSSION

Mutation of side chains that form hydrogen bonds with the internal water chain affects cytochrome *f* function. All mutations to water chain residues reduced the growth rate of *C. reinhardtii*, and the N168F replacement resulted in a loss of phototrophism (Table 4). All mutations also altered the $E_m$ of the protein, illustrating the fact that the fine atomic arrangement of the water chain region and hydrogen bonding of one of the waters by the heme ligand His25 are important for the precise setting of the $E_m$ in the wild-type protein (Table 3). All mutations resulting in a phototrophic phenotype also reduced the rate of cytochrome *f* reduction in vivo (Table 4).

Changes caused by mutagenesis of water chain residues are large relative to changes caused by mutagenesis at other sites in *C. reinhardtii* cytochrome *f*. We use as a basis for comparison other mutant forms of *C. reinhardtii* cytochrome *f*, in which two to five basic Lys side chains were replaced

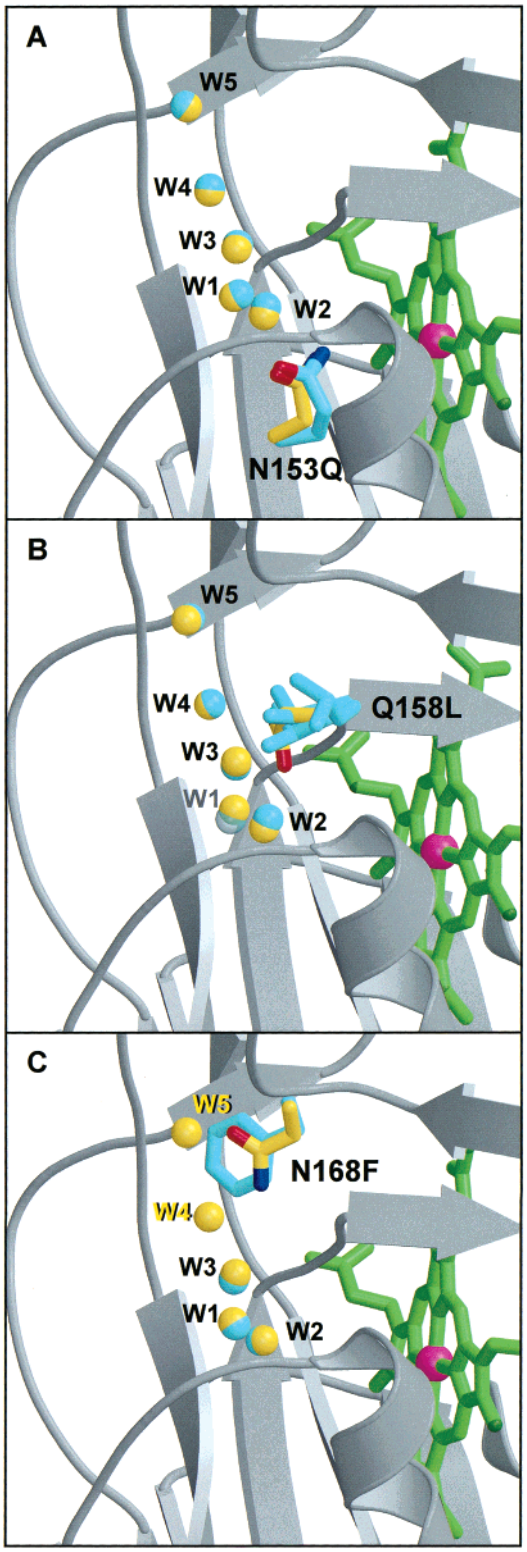


FIGURE 3: Single-site "water" mutants of cytochrome *f* affecting function of the protein: (A) N153Q, (B) Q158L [the more weakly bound water (W1) in this mutant is rendered as a translucent sphere with gray label], and (C) N168F. [Positions where waters have been displaced in this mutant (W4 and W5) are labeled in yellow.] For each mutant protein, the substituted side chain (cyan C) is shown with the wild-type side chain (yellow C), based on superposition of $C_\alpha$ atoms in the large domains. The protein backbone is rendered as a gray ribbon; the heme is green with pink Fe, and side chain O atoms are red and N atoms blue. Water O atoms are yellow in the wild type and cyan in the mutants.

Table 6: Structural Similarity of the Internal Water Chain in Wild-Type and Mutant Cytochromes

| | | N153Q | | Q158L | | N168F | |
|---|---|---|---|---|---|---|---|
| water | WT internal[a] | vs WT[b] | internal | vs WT | internal | vs WT | internal |
| W1 | 0.34 | 0.20 | 0.32 | 0.40 | 0.84 | 0.13 | 0.10 |
| W2 | 0.18 | 0.32 | 0.15 | 0.38 | 0.40 | 0.14 | 0.14 |
| W3 | 0.24 | 0.23 | 0.13 | 0.29 | 0.44 | 0.27 | 0.28 |
| W4 | 0.53 | 0.11 | 0.08 | 0.02 | 0.38 | not present | |
| W5 | 0.44 | 0.07 | 0.30 | 0.25 | 0.52 | not present | |

[a] Average discrepancy (angstroms) in water positions of redundant molecules in each crystal structure following superposition of large-domain $C_\alpha$ atoms. [b] Distance between water positions in mutant and wild-type cytochromes at each of the five sites. An average water position in each crystal structure was used for this calculation.

with neutral or acidic side chains (*12*, *13*). The Lys replacements eliminated a basic surface patch, which was thought to direct cytochrome *f* interactions with plastocyanin in vivo. For the replacements of as many as five Lys side chains, *C. reinhardtii* doubling times increased 10−40%, $E_m$ was reduced up to 10 mV, and the in vivo cytochrome *f* re-reduction half-time was increased 1.3−1.5-fold. By comparison, the single-site water chain replacements had much greater effects on cytochrome *f* function. *C. reinhardtii* doubling times increased 40−90% (and N168F was non-phototrophic); $E_m$ was reduced 30−80 mV, and the in vivo cytochrome *f* re-reduction half-time was increased 5−6-fold (ref *10* and this work).

*Structural Integrity of Water Chain Mutants.* The structures of the water chain mutant cytochromes are identical overall to the wild-type structure (Table 5). Perturbations to the structures were confined to the immediate vicinity of each substitution. All three mutants (N153Q, Q158L, and N168F) folded and assembled with heme at the same levels as the wild-type cytochrome in an *E. coli* expression system. Thus, the impairment of cytochrome function in vivo and the altered properties detected in vitro are not due to instability or gross rearrangements of the protein structure in the mutants. Residue 153 is the only one of the mutagenized residues in contact with the heme. The hydrogen bonding of mutant Gln153 and wild-type Asn153 are identical, but the heme contacts of the longer Gln153 side chain are more numerous than those of Asn153. Small changes in the heme electronic environment may account for the slightly altered properties of N153Q cytochrome *f*.

By far, the largest perturbation to any of the structures was the elimination of two waters (W4 and W5) from the internal five-water chain in the N168F mutant cytochrome. The Q158L substitution resulted in lower occupancy and shifted position for the water nearest residue 158 (W1). Both the N168F and Q158L substitutions resulted in loss of hydrogen bonds and diminished polarity of the water chain environment.

Two external water molecules near W5 have been proposed as part of the water chain (*4*). However, the external waters, like others in the first hydration shell of the protein, are more weakly bound than the internal waters with temperature factors more than twice those of W1−W5. We do not consider these external waters to be part of the water chain.

*Correlation of in Vivo and in Vitro Observations.* The greatest effects in vivo were seen for substitutions that altered

the structure of the water chain itself. N168F cytochrome *f* lost two waters from the internal chain and did not grow phototrophically. Among the phototrophic water mutants, Q158L had reduced occupancy and significantly altered position at one water site and was most severely impaired (*C. reinhardtii* doubling time increased 90%; cytochrome *f* re-reduction half-time increased 6-fold). We conclude from all the data that the internal five-water chain is important to cytochrome *f* function, and that perturbation of the water chain impairs function.

While there is a clear correlation between changes to the structure of the water chain and in vivo measurements of cytochrome *f* function, the picture is less clear for measurements that we can make in vitro. The spectral parameters, midpoint potentials, and rates of oxidation by plastocyanin do not correlate with loss of function in vivo or with changes to the internal water structure for the cytochrome *f* water mutants. It is likely that changes to the internal water structure impair a feature of cytochrome *f* function that is not accessible to in vitro measurements. The likeliest candidate is the reduction of cytochrome *f* by the Rieske protein, which has the largest changes among the in vivo assays. The in vivo kinetic measurements were made in a system with a fully reduced electron transfer pathway from PS II through cytochrome $b_6f$ to PS I. A flash of light triggered electron transfer from PS I to $NADP^+$, and subsequent electron flow through the entire pathway. Cytochrome *f* was initially oxidized by plastocyanin and then re-reduced by the Rieske protein. In this assay, changes to electron transfer rates through cytochrome *f* may have been masked by other slower steps in the pathway. Nevertheless, in the water mutants substantial changes were observed in the rate of cytochrome *f* re-reduction by the Rieske protein. This step has not yet been assayed effectively in vitro.

*Loss of Phototrophic Growth in N168F.* Low levels of N168F holocytochrome *f* in *C. reinhardtii* were either a result or cause of the loss of photosynthetic growth in this mutant. The content of wild-type and mutant holocytochrome *f* was estimated by heme staining of membranes from *C. reinhardtii* (*10*). Heme staining of protein in whole-cell extracts from late-log phase cultures of the N168F mutant revealed low levels of assembled cytochrome *f*. No detectable N168F cytochrome *f* was reported previously (*10*), but repeated determinations revealed low levels of 10−20% of the wild-type level (data not shown). These levels are at the threshold for sustaining photosynthetic growth with wild-type cytochrome *f* (*26*). Levels of Q158L cytochrome *f* in *C. reinhardtii* were 50−60% of the wild-type levels (*10*). Holocytochrome *f* was detected at the wild-type level in the N153Q mutant. The low steady state level of assembled cytochrome *f* in the N168F strain of *C. reinhardtii* is somewhat puzzling because (i) yields of N168F and wild-type proteins were identical in the *E. coli* expression system; (ii) the redox and spectroscopic characteristics of N168F differed no more from those of the wild type than did those of the Q158L and N153Q mutants, which were present at much higher levels in *C. reinhardtii*; and (iii) the $b_6f$ complex accumulates to almost wild-type levels in non-phototrophic mutants affecting subunit IV, the *petD* gene product (*27*). The low level of N168F cytochrome *f* in *C. reinhardtii* may have resulted from a defect not detected in the *E. coli* expression system. For example, the impaired function due to loss of two of the internal waters may have resulted in a higher rate of turnover of nonfunctional cytochrome $b_6f$, and/or a slower rate of cytochrome *f* assembly, which could then be subject to proteolytic degradation in vivo. Slow assembly of the $b_6f$ complex may also have caused an accumulation of unassembled cytochrome *f*, which can lead to inhibited translation of *petA* mRNA encoding cytochrome *f* (*28*).

*Proton Transfer Function (pK) of $E_m$ in the Wild Type and Mutants.* Proton transfer is an obvious function for the unique elongated buried water chain in cytochrome *f*. If a portion of this water chain is near the *p*-side membrane interface of the proton-translocating cytochrome $b_6f$ complex, then the water chain may function in the *p*-side exit port for protons translocated across the membrane by the complex. More specifically, we have suggested that the water chain may function in translocation of the second proton released on the *p* side of the $b_6f$ complex in the oxidation of plastoquinol, $PQH_2$ (*29*). The occurrence of proton-coupled electron transfer in cytochrome *f* is consistent with the diminished rate of cytochrome *f* reduction in mutants affecting residues that form hydrogen bonds with the water chain (*10*). The $E_m$ of cytochrome *f* is pH-independent from pH 4.5 to 8.0, with an observed p*K* at approximately pH 8.5. An obvious group in the heme vicinity that may be responsible for this p*K* is $N_{\delta 1}$ of His25 (2). The heme propionates are not in a hydrophobic environment, and have p*K*s below pH 5 in the aqueous phase (*30*). However, the hydroxyl groups of solvent-exposed tyrosine side chains near the heme, such as Tyr1, Tyr9, and Tyr160, could account for the high p*K*. The p*K* also could be due to one of the water molecules in the internal chain. Whatever group is responsible for the transition is unlikely to serve in physiological proton translocation at the low ambient pH of the chloroplast lumen, thus presenting a problem for the hypothesis of coupled electron and proton transfer in cytochrome $b_6f$.

## ACKNOWLEDGMENT

We thank R. Malkin, R. Kuras, L. Thöny-Meyer, and F.-A. Wollman for kindly providing materials used in the experiments described here and C. Greski for expert preparation of the manuscript.

## NOTE ADDED IN PROOF

While this paper was in press, a *C. reinhardtii* cytochrome *f* structure, which we cite in preliminary form (*4*), was published (*31*). The $P2_12_12_1$ crystal form reported is identical to that of the wild type and the N153Q and Q158L mutant cytochromes reported here. An intermolecular association in the crystal lattice is proposed by Berry and co-workers as a possible dimerization interface for cytochrome *f* in the dimeric cytochrome $b_6f$ complex. While this intermolecular contact buries a large cytochrome surface area, it also buries more than 15 water molecules in our wild-type cytochrome structure and in this respect resembles a crystal lattice contact more than a dimeric subunit interface. However, a similar lattice contact occurs in our structure of the N168F mutant cytochrome, which crystallized under nearly identical conditions in an unrelated ($P2_1$) form. The angle between molecules of the interacting pair differs by 8° in the N168F cytochrome (space group $P2_1$) and the other *C. reinhardtii*

cytochrome structures (space group $P2_12_12_1$). The intermolecular contact is not a general feature of cytochromes *f*, as it does not occur for one-third of the molecules in the $P2_12_12_1$ crystal form, and does not occur in the structures of either the turnip (*1*) or the cyanobacterial (*3*) cytochrome. As pointed out by Berry and co-workers, the heme orientation relative to the membrane plane that is inferred from the proposed dimeric arrangement of cytochrome *f* is inconsistent with EPR data on cytochrome $b_6f$ in oriented membranes.

## REFERENCES


1. Martinez, S. E., Huang, D., Szczepaniak, A., Cramer, W. A., and Smith, J. L. (1994) Crystal structure of the chloroplast cytochrome *f* reveals a novel cytochrome fold and unexpected heme ligation, *Structure 2*, 95−105.
2. Martinez, S. E., Huang, D., Ponomarev, M. V., Cramer, W. A., and Smith, J. L. (1996) The heme redox center of chloroplast cytochrome *f* is linked to a buried five-water chain, *Protein Sci. 5*, 1081−1092.
3. Carrell, C. J., Schlarb, B. G., Bendall, D. S., Howe, C. J., Cramer, W. A., and Smith, J. L. (1999) Structure of the soluble domain of cytochrome *f* from the cyanobacterium, *Phormidium laminosum*: convergent evolution of the membrane-bound *c*-type cytochromes from photosynthetic and respiratory cytochrome *bc* complexes, *Biochemistry 38*, 9590−9599.
4. Berry, E. A., Huang, L.-S., Chi, Y., Zhang, Z., Malkin, R., and Fernandez-Velasco, J. G. (1997) The crystallization and structure of a soluble form of *Chlamydomonas reinhardtii* cytochrome *f*, *Biophys. J. 72*, A125.
5. Ko, K., and Straus, N. A. (1987) Sequence of apocytochrome *f* gene encoded by the *Vicia faba* chloroplast genome, *Nucleic Acids Res. 15*, 2391−2394.
6. Kowalick, K. V., Stoebe, B., Schaffran, I., Kroth-Pancic, P., and Freier, U. (1995) The chloroplast genome of a chlorophyll *a*+*c*-containing alga, *Odontella sinensis*, *Plant Mol. Biol. Rep. 13*, 336−342.
7. Williams, M. A., Goodfellow, J. M., and Thornton, J. M. (1994) Buried waters and internal cavities in monomeric proteins, *Protein Sci. 3*, 1224−1235.
8. Luecke, H., Schobert, B., Richter, H. T., Cartailler, J. P., and Lanyi, J. K. (1999) Structural changes in bacteriorhodopsin during ion transport at 2-Å resolution, *Science 286*, 255−261.
9. Smirnova, I. A., Adelroth, P., Gennis, R. B., and Brzezinski, P. (1999) Aspartate-132 in cytochrome *c* oxidase from *Rhodobacter sphaeroides* is involved in a two-step proton transfer during oxo-ferryl formation, *Biochemistry 38*, 6826−6833.
10. Ponamarev, M. V., and Cramer, W. A. (1998) Perturbation of the internal water chain in cytochrome *f* of oxygenic photosynthesis: loss of the concerted reduction of cytochromes *f* and $b_6$, *Biochemistry 37*, 17199−17208.
11. Kuras, R., Wollman, F. A., and Joliot, P. (1995) Conversion of cytochrome *f* to a soluble form *in vivo* in *Chlamydomonas reinhardtii*, *Biochemistry 34*, 7468−7475.
12. Soriano, G. M., Ponamarev, M. V., Tae, G.-S., and Cramer, W. A. (1996) Effect of the interdomain basic region of cytochrome *f* on its redox reactions *in vivo*, *Biochemistry 35*, 14590−14598.
13. Soriano, G. M., Ponamarev, M. V., Piskorowski, R., and Cramer, W. A. (1998) Identification of the basic residues of cytochrome *f* responsible for electrostatic docking interactions with plastocyanin *in vitro*: relevance to the electron-transfer reaction *in vivo*, *Biochemistry 37*, 15120−15128.
14. Ponamarev, M. V., Schlarb, B. G., Carrell, C. J., Howe, C. J., Smith, J. L., Bendall, D. S., and Cramer, W. A. (2000) Trptyphan-heme $\pi$-electrostatic interactions in cytochrome *f* of oxygenic photosynthesis, *Biochemistry 39* (in press).
15. Thöny-Meyer, L., Fischer, F., Kunzler, P., Ritz, D., and Hennecke, H. (1995) *Escherichia coli* genes required for cytochrome *c* maturation, *J. Bacteriol. 177*, 4321−4326.
16. Metzger, S. U., Cramer, W. A., and Whitmarsh, J. (1997) Critical analysis of the extinction coefficient of chloroplast cytochrome *f*, *Biochim. Biophys. Acta 1319*, 233−241.
17. Westbrook, E. M., and Naday, I. (1997) Charge-coupled device-based area detectors, *Methods Enzymol. 276*, 244−268.
18. Otwinowski, Z. (1993) Oscillation data reduction program, in *Data Collection and Processing, Proceedings of the CCP4 Study Weekend, 29−30 January 1993* (Sawyer, L., Isaacs, N., and Bailey, S., Eds.) pp 56−62, SERC Laboratory, Daresbury, Warrington, England.
19. Otwinowski, Z., and Minor, W. (1997) Processing of X-ray Diffraction Data Collected in Oscillation Mode, *Methods Enzymol. 276*, 307−326.
20. Navaza, J. (1994) AMoRe: an automated package for molecular replacement, *Acta Crystallogr. A50*, 157−163.
21. Navaza, J., and Saludjian, P. (1997) AMoRe: An Automated Molecular Replacement Program Package, *Methods Enzymol. 276*, 581−594.
22. Jones, T. A., Zou, J.-Y., Cowan, S. W., and Kjeldgaard, M. (1991) Improved methods for building protein models in electron density maps and the location of errors in these models, *Acta Crystallogr. A47*, 110−119.
23. Brünger, A. T., Adams, P. D., Clore, G. M., DeLano, W. L., Gros, P., Grosse-Kunstleve, R. W., Jiang, J.-S., Kuszewski, J., Nilges, M., Pannu, N. S., Read, R. J., Rice, L. M., Simonson, T., and Warrem, G. L. (1998) Crystallography & NMR System: A New Software Suite for Macromolecular Structure Determination, *Acta Crystallogr. D54*, 905−921.
24. Collaborative Computational Project, Number 4 (1994) The CCP4 suite: programs for protein crystallography, *Acta Crystallogr. D50*, 760−763.
25. Clark, W. M. (1960) *Oxidation−Reduction Potentials of Organic Systems*, pp 180−182, Williams and Wilkins Co., Baltimore.
26. Chen, X., Kindle, K. L., and Stern, D. B. (1995) The initiation codon determines the efficiency but not the site of translation initiation in *Chlamydomonas* chloroplasts, *Plant Cell 7*, 1295−1305.
27. Zito, F., Finazzi, G., Delosme, R., Nitschke, W., Picot, D., and Wollman, F.-A. (1999) The $Q_o$ site of cytochrome $b_6f$ complexes controls the activation of the LHCII kinase, *EMBO J. 18*, 2961−2969.
28. Choquet, Y., Stern, D. B., Wostrikoff, K., Kuras, R., Girard-Bascou, J., and Wollman, F.-A. (1998) Translation of cytochrome *f* is autoregulated through the 5′ untranslated region of *petA* mRNA in *Chlamydomonas* chloroplasts, *Proc. Natl. Acad. Sci. U.S.A. 95*, 4380−4385.
29. Soriano, G. M., Ponamarev, M. V., Carrell, C. J., Xia, D., Smith, J. L., and Cramer, W. A. (1999) Comparison of the Cytochrome $bc_1$ Complex with the Anticipated Structure of the Cytochrome $b_6f$ Complex: De Plus Ça Change de Plus C'est la Même Chose, *J. Bioenerg. Biomembr. 31*, 201−213.
30. Moore, G. R., and Pettigrew, G. W. (1990) in *Cytochromes c*, pp 255−307, Springer-Verlag, New York.
31. Chi, Y.-I., Huang, L.-S., Zhang, Z., Fernández-Velasco, J. G., and Berry, E. A. (2000) *Biochemistry 39*, 7689−7701.


BI0004596